doi:10.1016/j.jmb.2009.10.009 *J. Mol. Biol.* (2009) **xx**, xxx–xxx

JMB

Available online at www.sciencedirect.com

ScienceDirect

ELSEVIER

Crystal Structures of the Histidine Acid Phosphatase from *Francisella tularensis* Provide Insight into Substrate Recognition

Harkewal Singh[1], Richard L. Felts[1], Jonathan P. Schuermann[2], Thomas J. Reilly[3] and John J. Tanner[1,4]*

[1]*Department of Chemistry, University of Missouri-Columbia, Columbia, MO 65211, USA*

[2]*Northeastern Collaborative Access Team, Department of Chemistry and Chemical Biology, Cornell University, Ithaca, NY 14853, USA*

[3]*Department of Veterinary Pathobiology and Veterinary Medical Diagnostic Laboratory, University of Missouri-Columbia, Columbia, MO 65211, USA*

[4]*Department of Biochemistry, University of Missouri-Columbia, Columbia, MO 65211, USA*

Received 9 September 2009; received in revised form 7 October 2009; accepted 8 October 2009

Edited by M. Guss

Histidine acid phosphatases catalyze the transfer of a phosphoryl group from phosphomonoesters to water at acidic pH using an active-site histidine. The histidine acid phosphatase from the category A pathogen *Francisella tularensis* (FtHAP) has been implicated in intramacrophage survival and virulence, motivating interest in understanding the structure and mechanism of this enzyme. Here, we report a structure-based study of ligand recognition by FtHAP. The 1.70-Å-resolution structure of FtHAP complexed with the competitive inhibitor L(+)-tartrate was solved using single-wavelength anomalous diffraction phasing. Structures of the ligand-free enzyme and the complex with inorganic phosphate were determined at resolutions of 1.85 and 1.70 Å, respectively. The structure of the Asp261Ala mutant enzyme complexed with the substrate 3′-AMP was determined at 1.50 Å resolution to gain insight into substrate recognition. FtHAP exhibits a two-domain fold similar to that of human prostatic acid phosphatase, consisting of an α/β core domain and a smaller domain that caps the core domain. The structures show that the core domain supplies the phosphoryl binding site, catalytic histidine (His17), and an aspartic acid residue (Asp261) that protonates the leaving group, while the cap domain contributes residues that enforce substrate preference. FtHAP and human prostatic acid phosphatase differ in the orientation of the crucial first helix of the cap domain, implying differences in the substrate preferences of the two enzymes. 3′-AMP binds in one end of a 15-Å-long tunnel, with the adenine clamped between Phe23 and Tyr135, and the ribose 2′-hydroxyl interacting with Gln132. The importance of the clamp is confirmed with site-directed mutagenesis; mutation of Phe23 and Tyr135 individually to Ala increases K_m by factors of 7 and 10, respectively. The structural data are consistent with a role for FtHAP in scavenging phosphate from small molecules present in host macrophage cells.

Keywords: histidine acid phosphatase; X-ray crystallography; kinetics; substrate recognition; *Francisella tularensis*

Introduction

Francisella tularensis is a highly infectious facultative intracellular bacterial pathogen and the causative agent of the potentially fatal disease tularemia.[1] Due to its high infectivity and lethality and the potential for use as a bioterrorism agent, the Centers for Disease Control and Prevention considers *F.*

**Corresponding author.* Department of Chemistry, University of Missouri-Columbia, Columbia, MO 65211, USA. E-mail address: tannerjj@missouri.edu.

Abbreviations used: HAP, histidine acid phosphatase; FtHAP, *Francisella tularensis* histidine acid phosphatase; hPAP, human prostatic acid phosphatase; rPAP, rat prostatic acid phosphatase; PDB, Protein Data Bank; P_i, inorganic phosphate; D261A, mutant of FtHAP in which Asp261 is replaced by Ala; F23A, mutant of FtHAP in which Phe23 is replaced by Ala; Y135A, mutant of FtHAP in which Tyr135 is replaced by Ala; *p*NPP, *p*-nitrophenyl phosphate; PEG, polyethylene glycol; Se-Met, selenomethionine.

0022-2836/$ - see front matter

Please cite this article as: Singh H. *et al.*, Crystal Structures of the Histidine Acid Phosphatase from *Francisella tularensis* Provide Insight into Substrate Recognition, *J. Mol. Biol.* (2009), doi:10.1016/j.jmb.2009.10.009

tularensis to be a category A agent. Currently, there is no licensed vaccine available, and new antibiotics are needed in anticipation of strains engineered to have enhanced virulence.

Acid phosphatases have been shown to be essential for intramacrophage survival and virulence of *F. tularensis*.[2,3] Four acid phosphatase genes have been identified in highly virulent type A strains: *acpA*, *acpB*, *acpC*, and *hap* (encodes the enzyme studied here). AcpA is the prototype of a unique superfamily of acid phosphatases and phospholipases C.[4] AcpB and AcpC[5] belong to the DDDD superfamily of phosphohydrolases.[6] The *hap* gene product is unrelated to the other three phosphatases. Real-time PCR analysis of gene expression in macrophages infected with *F. tularensis* subsp. *novicida* showed that the *acpA* and *hap* genes are induced 219- and 10-fold, respectively, upon infection, indicating that the intracellular environment activates these genes.[3] Furthermore, a triple mutant strain of *F. novicida* lacking functional *acpA*, *acpC*, and *hap* genes is defective for survival inside macrophages and exhibited a marked defect in time to death in a mouse model of tularemia.[3] Moreover, mice infected with a quadruple mutant lacking all four acid phosphatase genes showed 100% survival at 9 weeks after infection, and this mutant showed promising protective capacity as a single-dose live vaccine.[3]

The demonstration that acid phosphatase activity is essential for intracellular survival and virulence of *F. tularensis* has generated new interest in understanding the structures and molecular functions of the four acid phosphatases. The enzymes encoded by *acpA*,[7] *acpC*,[5] and *hap*[8] have been crystallized, and the structure of AcpA has been determined.[4] Also, kinetic and biophysical studies of AcpA have been reported.[9,10]

Herein, we present a structure-based study of the *hap* gene product [*F. tularensis* histidine acid phosphatase (FtHAP)] focused on substrate recognition. FtHAP is a 37-kDa periplasmic acid phosphatase that contains the characteristic histidine acid phosphatase (HAP) sequence motif of RHGXRXP, which was first identified in human prostatic acid phosphatase (hPAP) by Van Etten *et al.*[11] Crystal structures of hPAP[12–14] and the rat homolog[15–17] [rat prostatic acid phosphatase (rPAP)] are known, but heretofore, the structure of a bacterial HAP has not been reported. In the following, we present four high-resolution crystal structures of FtHAP (Table 1), including structures of the enzyme complexed with the product inorganic phosphate (P_i) and the competitive inhibitor L(+)-tartrate, as well as the first structure of a HAP/substrate complex. The data provide insight into the structural determinants of substrate recognition by FtHAP and other HAPs.

Table 1. Data collection and refinement statistics

Enzyme	Se-Met	Native	Native	Native	D261A
Active-site ligand	L(+)-Tartrate	Phosphate	L(+)-Tartrate	None	3′-AMP
Space group	$P4_12_12$	$P4_1$	$P4_1$	$P4_1$	$P4_1$
Unit cell lengths (Å)	$a=61.9$, $c=210.9$	$a=61.9$, $c=211.6$	$a=62.0$, $c=210.9$	$a=62.4$, $c=209.9$	$a=61.6$, $c=211.4$
Wavelength	0.979091	1.00000	1.12711	1.12711	0.97918
Resolution (Å)	43.79–2.10 (2.18–2.10)	34.95–1.70 (1.76–1.70)	46.51–1.70 (1.76–1.70)	40.17–1.85 (1.92–1.85)	33.63–1.50 (1.55–1.50)
No. of observations	338,002	351,571	262,561	231,368	938,410
No. of unique reflections	25,062	86,186	79,753	67,426	125,320
R_{merge} (I)	0.094 (0.338)	0.095 (0.249)	0.067 (0.384)	0.077 (0.290)	0.074 (0.539)
Average I/σ	15.2 (7.3)	8.4 (2.9)	12.7 (2.2)	10.0 (2.2)	32.3 (2.8)
Completeness (%)	100.0 (100.0)	99.0 (95.1)	91.7 (84.6)	99.1(99.7)	99.9 (100.0)
Redundancy	13.49 (14.38)	4.08 (3.12)	3.29 (2.66)	3.43 (2.76)	7.5 (7.4)
R_{cryst}		0.189	0.184	0.203	0.172
R_{free}[a]		0.215	0.207	0.227	0.187
No. of protein residues		658	657	656	672
No. of protein atoms		5099	5129	5096	5295
No. of water molecules		516	413	283	580
Average B-factor (Å^2)					
Protein		27.6	28.2	32.9	19.9
Water		34.6	33.6	36.0	28.3
Active-site ligand		25.1	20.5		18.4
rmsd[b]					
Bond lengths (Å)		0.004	0.007	0.006	0.005
Bond angles (°)		0.91	1.03	0.89	0.98
Ramachandran plot (%)[c]					
Favored		99.24	99.23	99.38	99.25
Allowed		0.76	0.77	0.62	0.75
Outliers		0	0	0	0
PDB accession code		3IT0	3IT1	3IT2	3IT3

Values for the outer resolution shell of data are given in parentheses.
[a] Five percent test set. A common set of test reflections was used for refinement of all structures.
[b] Compared to the parameters of Engh and Huber.[18]
[c] The Ramachandran plot was generated with RAMPAGE.[19]

Please cite this article as: Singh H. *et al.*, Crystal Structures of the Histidine Acid Phosphatase from *Francisella tularensis* Provide Insight into Substrate Recognition, *J. Mol. Biol.* (2009), doi:10.1016/j.jmb.2009.10.009

Results

Structure of the FtHAP protomer

The FtHAP protomer comprises two domains and has approximate dimensions of 60 Å×32 Å×30 Å. The core domain is a twisted, seven-stranded β-sheet flanked by two α-helices on one side and three on the other side (Fig. 1a). The strand order of the β-sheet is 3, 2, 4, 1, 5, 6, and 7, with all but strands 5 and 7 in parallel. This domain is similar to the α/β core domains of enzymes in the histidine phosphatase superfamily[21] and thus identifies FtHAP as a member of this group. The second domain (Fig. 1b, pink) caps the core domain and consists of two sections of the polypeptide chain that are inserted between secondary structural elements of the core domain. The first insertion follows β1 and consists of a loop formed by residues 21–38. The second insertion follows β3 and includes residues 134–222, which form a bundle of α-helices.

The active site is located in the junction of the two domains, at one end of a solvent-filled tunnel that runs through the protein, as indicated by the bound P_i anion in Fig. 1a and b. The core domain contributes the presumptive catalytic histidine residue (His17) and other residues that form the phosphoryl-binding pocket, which is located in the floor of the tunnel. The cap domain forms the walls and ceiling of the tunnel. As shown below, residues of the cap domain are important for binding the non-phosphoryl groups of the substrate 3′-AMP, implying that this domain plays a role in enforcing substrate preference.

hPAP[12–14] is the closest structural homolog of FtHAP, based on a query of the Protein Data Bank (PDB) with Secondary-Structure Matching.[22] The rmsd between the two enzymes is 1.7 Å over 273 residues (out of 329), despite sharing only 27% amino acid sequence identity. The superposition of FtHAP and hPAP shown in Fig. 2a confirms that the two enzymes share a common fold. There is, however, a major difference in the orientation of the first helix of the cap domain (α3, colored red in Fig. 2). The corresponding helix of hPAP (colored yellow in Fig. 2) is shifted 12 Å away from the active site compared to FtHAP. This difference appears to be due to a disulfide bond in hPAP that links residue 129 at the N-terminus of this helix with residue 340 near the C-terminus of the polypeptide chain (Fig. 2b). These Cys residues are absent in FtHAP, which evidently allows α3 to sit closer to the phosphoryl binding site. Consequently, the active-site entrance is narrower in FtHAP than in hPAP.

Structure of the dimer

FtHAP forms a dimer in solution based on gel filtration and sedimentation equilibrium studies (data not shown), and the two-molecule assembly in the asymmetric unit (Fig. 3) likely represents this dimer. This assembly has an interface area of 1600 $Å^2$ and a complexation significance score of

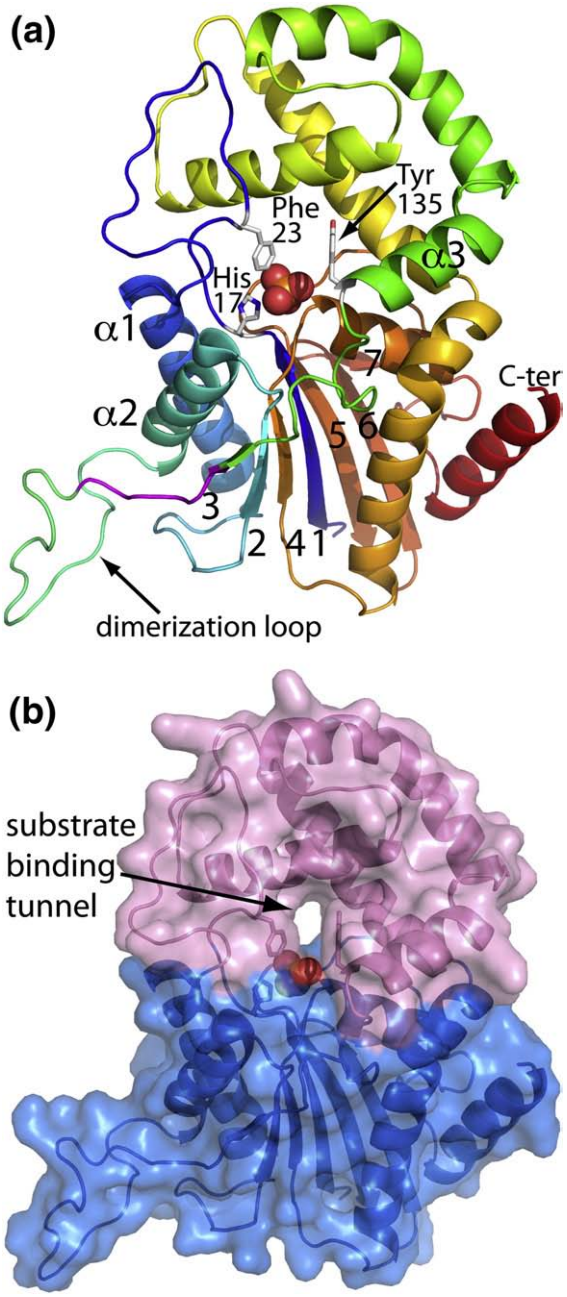

Fig. 1. Overall fold of FtHAP. (a) Ribbon drawing of the FtHAP protomer. Residues are colored according to a rainbow scheme, with blue at the N-terminus and red at the C-terminus. The P_i ligand is shown in spheres. The side chains of His17, Phe23, and Tyr135 are drawn as sticks in white. Strands of the β-sheet are numbered. The first three helices of the polypeptide chain are labeled α1, α2, and α3. The conserved portion of the dimerization loop (residues 116–121) is colored magenta. (b) Ribbon and surface representations of the protomer, highlighting domain structure. The orientation is the same as in (a). The core domain is colored blue, and the cap domain is colored pink. The P_i ligand is shown in spheres, and the side chains of His17, Phe23, and Tyr135 are drawn as sticks. This figure and others were created with PyMOL.[20]

Please cite this article as: Singh H. *et al.*, Crystal Structures of the Histidine Acid Phosphatase from *Francisella tularensis* Provide Insight into Substrate Recognition, *J. Mol. Biol.* (2009), doi:10.1016/j.jmb.2009.10.009

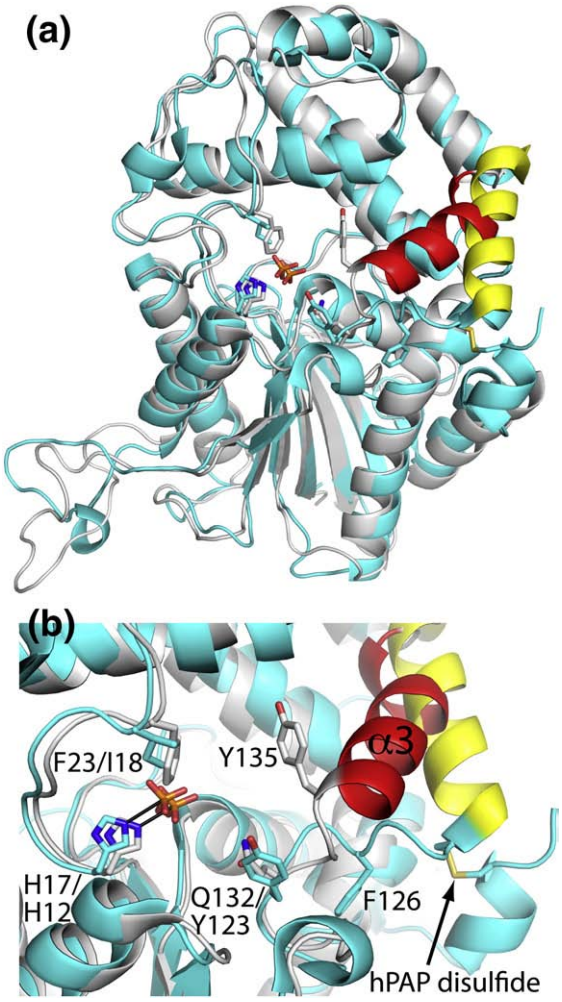

Fig. 2. Comparison of FtHAP and hPAP. (a) Ribbon drawings of FtHAP (white) and hPAP (cyan, PDB code: 1ND6) complexed with P_i. Helix α3 of FtHAP is colored red. The corresponding helix of hPAP is colored yellow. (b) Close-up view of the active sites using the same coloring scheme as in (a). Where appropriate, residue numbers are listed as FtHAP/hPAP.

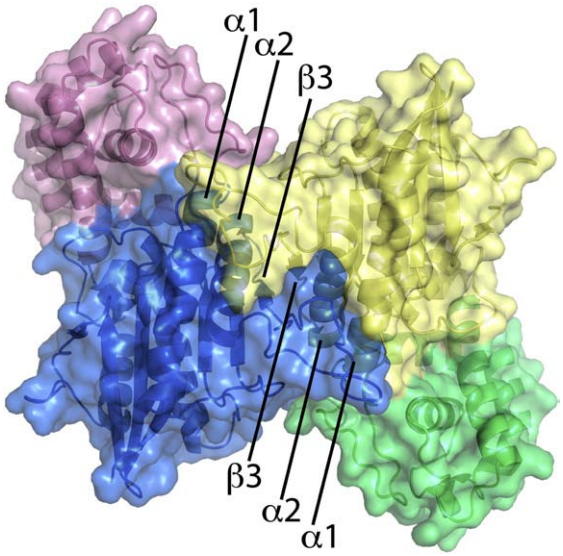

Fig. 3. Dimer structure of FtHAP. The core domains of the two protomers are colored blue and yellow. The cap domains are colored pink and green. The blue/pink protomer is related to the one in Fig. 1b by an approximate rotation of 180° around the vertical axis. Secondary structural elements that contribute to the dimer interface are indicated.

1.0, based on analysis with PISA.[23] The next largest interface in the lattice buries only 400 Å^2 of surface area, and the complexation significance score is 0.0. Furthermore, an identical dimer is present in the crystal lattices of the close structural homologs hPAP and rPAP.

The FtHAP dimer comprises two interlocking protomers (Fig. 3). A prominent feature of the dimer is the long, protruding loop that connects α2 and β3 of the core domain (residues 98–121, Fig. 1a). This loop reaches out and embraces the core domain of the other protomer, thus forming an interlocking dimer. Additional secondary structural elements buried in the dimer interface include α1, α2, and β3 (Fig. 3).

Structure of FtHAP complexed with P_i

The structure of FtHAP complexed with the product P_i was determined at 1.70 Å resolution (Table 1). This complex provides information about the identities of residues that directly participate in catalysis as well as those stabilizing the phosphoryl group of phosphomonoester substrates. The ion interacts with Arg16, His17, Arg20, Arg84, His260, Asp261, and one water molecule (Fig. 4a). Note that Arg16, His17, and Arg20 are part of the conserved RHGXRXP signature motif.

The oxygen atom of P_i denoted by O1 in Fig. 4a likely represents the O atom of the scissile P–O bond of the substrate or, equivalently, an O atom derived from the water molecule that attacks the phosphoenzyme intermediate. While the other oxygen atoms of P_i are buried in the active site, the P–O1 bond is directed toward the protein surface. Furthermore, O1 is the only oxygen atom of P_i that interacts with Asp261, a conserved residue proposed by Van Etten's group to protonate the leaving group.[24,25]

The FtHAP/P_i structure is consistent with His17 being the enzyme nucleophile. His17 forms the closest contact between the protein and the P atom (3.0 Å). Furthermore, the angle formed by the ε2 nitrogen atom of His17, the P atom, and O1 is approximately 180°, which is consistent with backside, in-line nucleophilic attack by His17. We note that the aforementioned interactions are essentially identical with those found in the structure of hPAP complexed with P_i (PDB code: 1nd6[14]).

Structure of FtHAP complexed with L(+)-tartrate

Inhibition by L(+)-tartrate is a common characteristic of HAPs, and as expected, L(+)-tartrate is a competitive inhibitor of FtHAP. The inhibition

Please cite this article as: Singh H. *et al.*, Crystal Structures of the Histidine Acid Phosphatase from *Francisella tularensis* Provide Insight into Substrate Recognition, *J. Mol. Biol.* (2009), doi:10.1016/j.jmb.2009.10.009

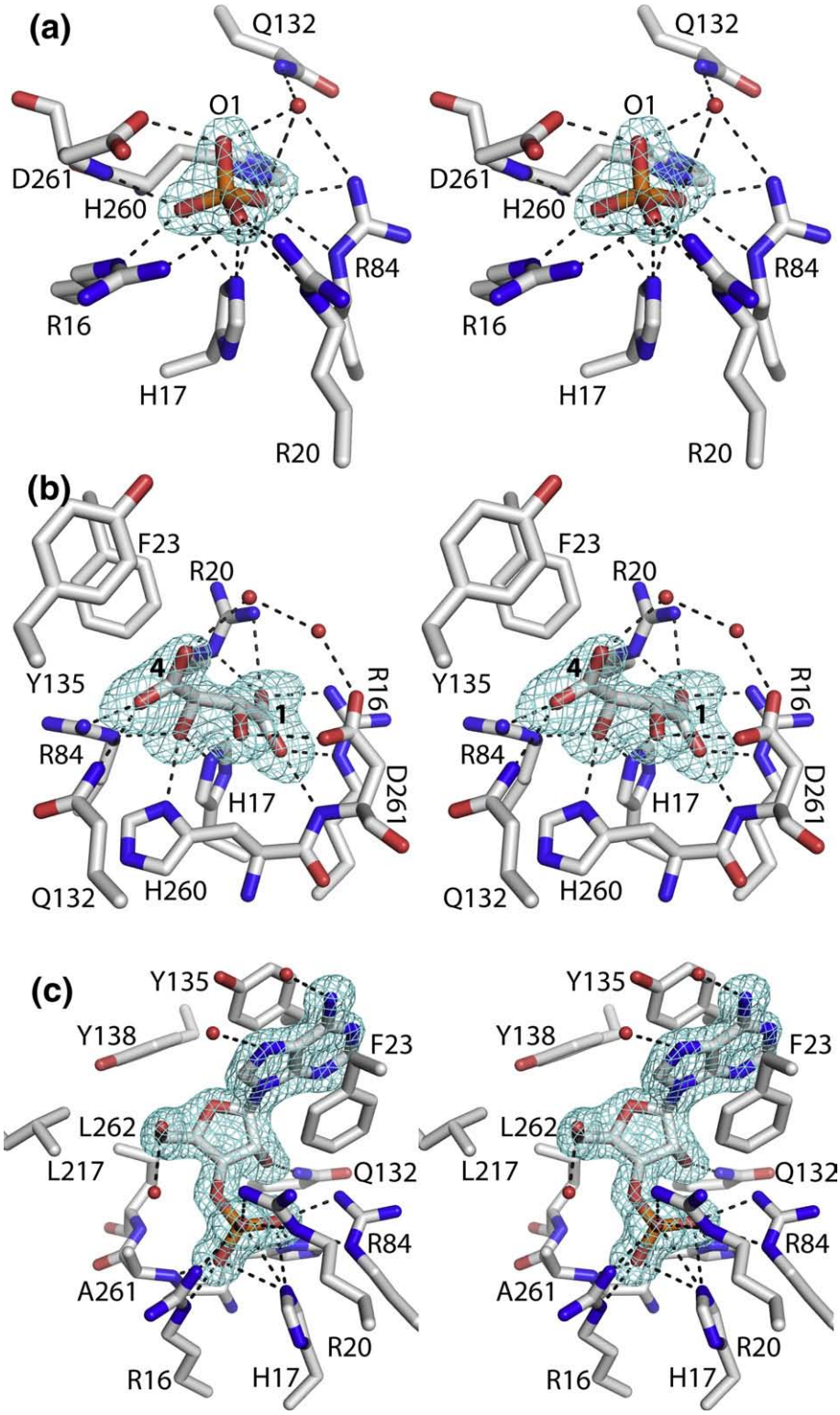

Fig. 4. Stereographic views (relaxed) of the active sites of (a) FtHAP complexed with P_i, (b) FtHAP complexed with L(+)-tartrate, and (c) FtHAP mutant D261A complexed with 3′-AMP. In each panel, the cage represents a simulated annealing σ_A-weighted $F_o - F_c$ map contoured at 3 σ. Prior to calculation of the map, the active-site ligand and surrounding side chains were omitted, and simulated annealing refinement was performed with PHENIX.

constant (K_i) is 0.2 mM, which is similar to the value of 0.15 mM reported for hPAP.[24] The 1.70-Å-resolution structure of FtHAP complexed with L(+)-tartrate is the first high-resolution structure of any HAP complexed with this inhibitor. A moderate resolution (2.9 Å) structure of hPAP complexed with the L(+)-tartrate analog *N*-propyl-L-tartramate has been reported (PDB code: 2HPA[13]).

The bound L(+)-tartrate anion interacts with eight residues, and every functional group of the inhibitor

Please cite this article as: Singh H. *et al.*, Crystal Structures of the Histidine Acid Phosphatase from *Francisella tularensis* Provide Insight into Substrate Recognition, *J. Mol. Biol.* (2009), doi:10.1016/j.jmb.2009.10.009

is engaged in at least one electrostatic interaction with the protein (Fig. 4b). One of the carboxylate groups (labeled 1 in Fig. 4b) is buried deep in the P_i site, where it interacts with the side chains of Arg16 and Arg20, as well as the backbone N–H group of Asp261. The adjacent hydroxyl group of the inhibitor occupies the P_i O1 binding site and forms a hydrogen bond with Asp261. The other hydroxyl group of the inhibitor forms hydrogen bonds with His17, His260, and Arg84. Presumably, His17—the catalytic residue—is a hydrogen-bond acceptor, while His260 and Arg84 are donors. Finally, the carboxylate group of the inhibitor distal from the P_i site (labeled 4 in Fig. 4b) interacts with Arg84 and Gln132. All of these enzyme–inhibitor interactions, except for the hydrogen bond with Gln132, are also observed in the hPAP/*N*-propyl-L-tartramate complex.

Structure of D261A complexed with 3′-AMP

How HAPs recognize the non-phosphoryl groups of substrates is a major outstanding question. According to our initial analysis of substrate preferences, FtHAP dephosphorylates a number of different phosphomonoesters, with 3′-AMP being one of the best substrates tested (Supplementary Fig. S1). Therefore, several site-directed mutants of FtHAP were created for use in structure determination of an enzyme/3′-AMP complex. D261A (mutant of FtHAP in which Asp261 is replaced by Ala) proved to be the most useful of these mutant enzymes for trapping 3′-AMP in the active site. The choice of D261A was motivated by analogous work on the protein tyrosine phosphatase PTP1B (unrelated in sequence and structure to HAPs), which showed that PTP1B mutant D181A is an effective substrate trap.[26] Asp181 of PTP1B is the general acid that protonates the substrate leaving group, and Asp261 is predicted to play this role in FtHAP based on studies of homologous HAP enzymes.[24,25]

The structure of D261A complexed with the *in vitro* substrate 3′-AMP (K_m = 0.3 mM, k_{cat} = 120 s^{-1}) was solved at 1.50 Å resolution (Table 1). The electron density maps clearly indicated the conformation of the substrate (Fig. 4c). 3′-AMP binds in one end of a tunnel of length 15 Å that is connected to the bulk medium at both ends (Fig. 5). One edge of the adenine base is exposed to the bulk medium, while the rest of the substrate is inside the tunnel (Fig. 5).

The environment of the 3′-AMP phosphoryl group is identical with that described for P_i above, except for the interaction with Asp261, which is obviously absent in D261A. Modeling of Asp261 based on the FtHAP/P_i complex suggests that this residue could potentially interact with the 3′ oxygen atom of 3′-AMP at a distance of 2.5 Å. Such an interaction is consistent with Asp261 functioning as the acid that protonates the leaving group.

The enzyme also interacts with the ribose moiety of the 3′-AMP (Fig. 4c). The 2′-hydroxyl interacts with Gln132 via a direct hydrogen bond and a water-mediated one. The 5′-hydroxyl does not directly interact with the enzyme, but it does form a hydrogen bond with a water molecule that is part of a network of hydrogen-bonded water molecules in the tunnel (Fig. 5).

The base of 3′-AMP stacks in parallel between the side chains of Phe23 and Tyr135, forming a sandwich (Figs. 4c and 5). The adenine is within van der Waals contact with the aromatic rings of these residues, indicating that the stacking is intimate. Note that the Watson–Crick hydrogen-bonding groups of the base are directed out of the tunnel toward the bulk medium. As a result, the base does not form hydrogen bonds with the enzyme. The adenine ring does interact with two water molecules via hydrogen bonding (Fig. 4c).

Finally, although all three groups of 3′-AMP—phosphoryl, ribose, and adenine—interact with the enzyme, the fit between this substrate and enzyme is not perfect. As shown in Fig. 5, the substrate does not completely fill the substrate-binding tunnel, implying suboptimal shape complementarity with 3′-AMP. In particular, the pocket has substantial available space around the ribose 5′-hydroxyl, which is directed toward the solvent-filled end of the tunnel.

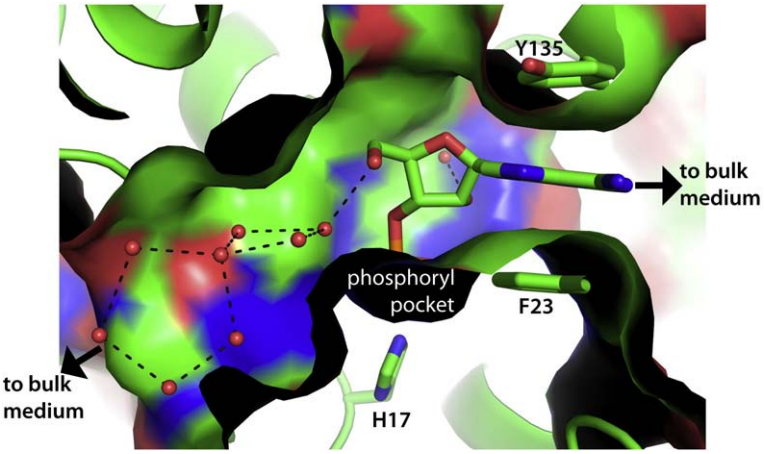

Fig. 5. Cutaway view of the substrate-binding tunnel with bound 3′-AMP.

Please cite this article as: Singh H. *et al.*, Crystal Structures of the Histidine Acid Phosphatase from *Francisella tularensis* Provide Insight into Substrate Recognition, *J. Mol. Biol.* (2009), doi:10.1016/j.jmb.2009.10.009

Analysis of conformational changes induced by ligand binding

The structure of inhibitor-free FtHAP was determined to gain insight into the conformational changes that accompany the binding of inhibitors and substrates. A superposition of the four FtHAP structures is shown in Fig. 6. The active sites are nearly identical, except for the conformations of Arg20, Phe23, and Tyr135.

The unique conformation of Arg20 in the ligand-free enzyme appears to be due to the presence of an acetate ion near this residue. (We note that sodium acetate was included in the enzyme storage buffer.) In the ligand-free enzyme, the bound acetate ion occupies the location corresponding to the phenyl group of Phe23 in the other structures. Electron density for the side chain of Phe23 was very weak in the ligand-free enzyme, indicating that this side chain is disordered. Note that Phe23 has been truncated after the C^{β} atom in the ligand-free enzyme structure.

The structural comparison also reveals perceptible differences involving the substrate-clamping residues Phe23 and Tyr135. These side chains are closest together in the 3′-AMP complex (Fig. 6, magenta). Furthermore, the electron density for these side chains is very strong in the 3′-AMP complex but comparatively weaker in the other structures. These observations suggest that the binding of 3′-AMP induces ordering of the side chains of Phe23 and Tyr135 and closure of the clamp.

Kinetic characterization of F23A and Y135A

The importance of the substrate-clamping residues was studied by creating the mutants F23A (mutant of FtHAP in which Phe23 is replaced by Ala) and Y135A (mutant of FtHAP in which Tyr135 is replaced by Ala). Steady-state kinetics measurements were performed using 3′-AMP as the substrate, and the resulting kinetic parameters are listed in Table 2.

Table 2. Kinetic parameters for native FtHAP, F23A, and Y135A using 3′-AMP as the substrate

	K_m (mM)	k_{cat} (s^{-1})	k_{cat}/K_m (s^{-1} mM^{-1})
Native	0.315±0.001	119.9±0.1	381
F23A	2.195±0.002	37.5±0.4	17
Y135A	3.0±0.5	93±31	31

The kinetic data suggest that Phe23 and Tyr135 play a significant role in binding 3′-AMP. The kinetic parameters for the native enzyme are 0.3 mM and 120 s^{-1} for K_m and k_{cat}, respectively, which yields a catalytic efficiency of 381 s^{-1} mM^{-1}. The efficiencies of F23A and Y135A are 20- and 10-fold lower, respectively. These decreases in efficiency reflect primarily changes in K_m, which increases from 0.3 mM for the native enzyme to 2.2 mM for F23A and 3.0 mM for Y135A. These results suggest that the stacking interactions implied by the crystal structure contribute substantially to the binding energy of 3′-AMP.

Discussion

FtHAP belongs to a large class of enzymes known as the histidine phosphatase superfamily.[21] This superfamily comprises phosphoryl transfer enzymes

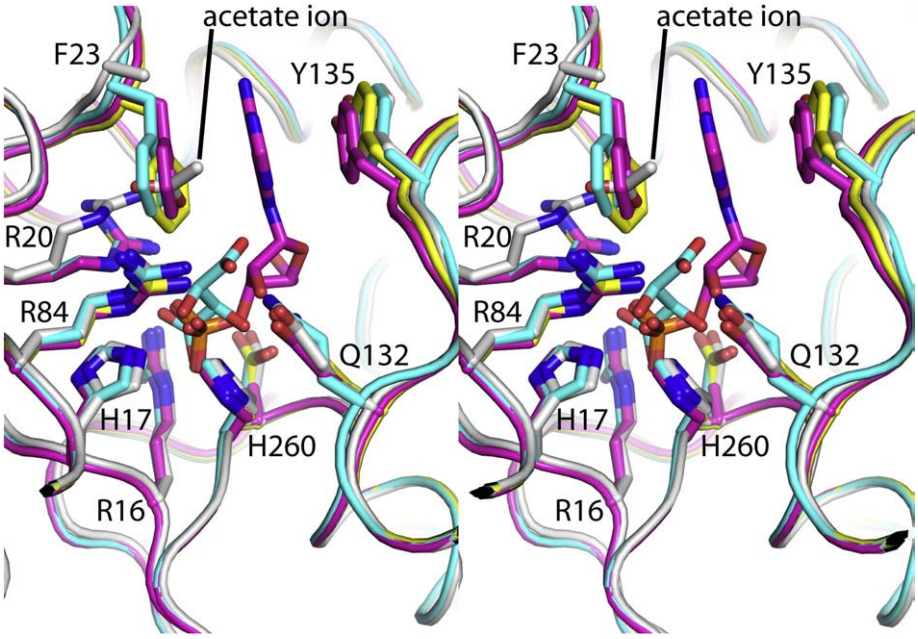

Fig. 6. Superposition (relaxed stereographic view) of the active sites of the four FtHAP structures. The complexes are colored as follows: inhibitor-free FtHAP, white; P_i complex, yellow; L(+)-tartrate complex, cyan; 3′-AMP complex, magenta.

Please cite this article as: Singh H. *et al.*, Crystal Structures of the Histidine Acid Phosphatase from *Francisella tularensis* Provide Insight into Substrate Recognition, *J. Mol. Biol.* (2009), doi:10.1016/j.jmb.2009.10.009

that share a common catalytic core featuring an active-site histidine that is phosphorylated during the catalytic cycle. There are two main branches in the superfamily, which are distinguished by sequence and structural characteristics. Branch 1 comprises several functionally diverse enzymes, including cofactor-dependent phosphoglycerate mutases and a variety of phosphatases. Branch 2 is less diverse and consists mainly of HAPs, such as FtHAP and hPAP, as well as phytases.

Here, we described the first structure of a bacterial member of the HAP subbranch of the histidine phosphatase superfamily. FtHAP has the same fold and dimeric structure as hPAP. The core catalytic domains of FtHAP and hPAP superimpose almost perfectly, which is consistent with the fact that the core domain is common to all members of the superfamily. It is thus likely that the fold displayed by FtHAP and hPAP is conserved throughout the HAP subbranch of the histidine phosphatase superfamily. Multiple sequence alignments suggest that the dimerization loop is present in other HAPs. Furthermore, the alignments reveal that seven residues near the end of the dimerization loop, corresponding to residues 116–121 of FtHAP, are highly conserved (colored magenta in Fig. 1a). This section of the loop has the sequence FQPIPI in FtHAP. The corresponding sequence in hPAP and many other predicted HAPs is WQPIPV. These observations suggest that the dimeric structure displayed by FtHAP and hPAP is also conserved throughout the HAP subbranch. Where FtHAP and hPAP differ is in the cap domain (pink in Fig. 1b), which we have shown is important for substrate recognition. In particular, the crucial first helix of the cap domain (α3) is shifted due to a disulfide bond that is present in hPAP but absent in FtHAP (Fig. 2b). This key structural difference in the active site implies that the two enzymes have different substrate preferences.

Although some of the physiological substrates for hPAP have been identified, nothing is known about the *in vivo* substrates for FtHAP. Previous work has suggested that the cellular form of hPAP functions as a protein phosphatase, with potential substrates including c-ErbB-2[27] and the epidermal growth factor receptor.[28] Also, the transmembrane isoform of hPAP has been recently shown to suppress pain by dephosphorylating extracellular 5′-AMP to adenosine.[29,30]

The structural data reported here provide clues about potential *in vivo* substrates and possible roles for FtHAP in intracellular survival. The active-site entrance of FtHAP is narrower than that of hPAP due to the difference in the orientation of α3 (Fig. 2b). The width of the active-site entrance could help dictate substrate specificity, with wider entrances allowing broader specificity, as has been suggested for PhoE, another member of the histidine phosphatase superfamily.[31] The wider entrance of hPAP is consistent with phosphoprotein substrates but evidently does not preclude 5′-AMP as a substrate. Conversely, the narrow entrance of FtHAP is predicted to preclude phosphoproteins as potential substrates and instead suggests small-molecule phosphomonoesters as potential substrates. In fact, docking of a phosphotyrosine pentapeptide into the FtHAP and hPAP structures suggests that residues flanking the phosphotyrosine would clash with α3 of FtHAP but not with the corresponding helix of hPAP (data not shown). Thus, our data argue against a role for FtHAP in modulating host cell signaling pathways by dephosphorylating host proteins.

The D261A/3′-AMP structure is the first structure of a substrate complex for any HAP, and thus, a major result of this work is to identify some of the structural determinants of substrate recognition by HAPs. In particular, the structure provides the first clues about residues that bind the non-phosphoryl groups of substrates. The structure shows that residues of the cap domain interact with the ribose and adenine, which suggests that the role of this domain is to help enforce substrate preference. The cap domain provides two main contact points with 3′-AMP. Primary among these is the first helix of the domain, which contains the key residues Gln132 and Tyr135. The former residue forms a hydrogen bond with the 2′-hydroxyl of 3′-AMP, while the latter forms one side of an aromatic sandwich that clamps the adenine base. The second locus of interaction is the large loop insertion that follows β1. This loop contributes Phe23, which forms the other side of the clamp. We thus propose that α3 and the large loop insertion are "hot spots" for substrate recognition.

It is interesting that Phe23, Gln132, and Tyr135 are not widely conserved among HAPs. Isoleucine and valine are frequently found at the residue corresponding to Phe23, with Ile appearing in hPAP, rPAP, and the closest sequence homolog to FtHAP in GenBank, *Legionella pneumophila* major acid phosphatase[32] (41% identity). The residues corresponding to Gln132 and Tyr135 display wide variation among HAPs. The *Legionella* enzyme appears to be the only other HAP having a glutamine aligning with FtHAP Gln132. Arginine substitutes for Tyr135 in the *Legionella* enzyme. The equivalent residues in hPAP and rPAP are Tyr123 and Phe126. Tyr123 of hPAP aligns structurally with FtHAP Gln132 (Fig. 2b); the hydroxyl group of Tyr123 could potentially play a role in substrate binding analogous to the carboxamide of FtHAP Gln132. On the other hand, Phe126 of the human enzyme is located 13 Å (C^{ζ}–C^{ζ} distance) from Tyr135 of FtHAP because of the shift in α3 discussed above (Fig. 2b). Thus, significant conformational change would be required to bring this residue of hPAP into the active site to bind substrates in the manner demonstrated by the D261A/3′-AMP structure. The lack of conservation of these key residues suggests that the substrate preference of FtHAP might be unique among HAPs.

Information about substrate recognition hot spots should aid the discovery of physiological substrates of FtHAP, which is important for understanding the enzyme's biological role. For example, gene deletion

Please cite this article as: Singh H. *et al.*, Crystal Structures of the Histidine Acid Phosphatase from *Francisella tularensis* Provide Insight into Substrate Recognition, *J. Mol. Biol.* (2009), doi:10.1016/j.jmb.2009.10.009

studies have implicated phosphatases, including FtHAP, in intramacrophage survival and virulence of *F. tularensis*, but a more detailed, molecular-level understanding of the biological roles of FtHAP, AcpA, AcpB, and AcpC is lacking. Our data provide some general ideas that might be useful in future studies intended to identify the biological function of FtHAP. For example, the D261A/3′-AMP structure shows that 3′-AMP perfectly spans the distance between the P_i binding site and the hydrophobic clamp. Thus, it appears that the active site is suited for binding nucleoside 3′-monophosphates. Since the enzyme does not form hydrogen bonds with the adenine base, FtHAP is predicted to lack a significant base preference for nucleoside 3′-monophosphates. Because 3′-AMP does not completely fill the substrate-binding tunnel, it is unlikely that the substrate preference of FtHAP is tightly restricted to nucleoside 3′-monophosphates. Indeed, initial *in vitro* kinetic screening trials also identified 2′- and 5′-nucleoside monophosphates as substrates for FtHAP (Supplementary Fig. S1). How the enzyme recognizes these substrates remains to be determined. Taken together, the structural data presented here point to a possible role for FtHAP in scavenging phosphate from small molecules present in host macrophage cells, perhaps with a preference for acquiring phosphate from nucleoside monophosphates.

Materials and Methods

Crystallization of native, Se-Met, and mutant FtHAP

Native FtHAP was expressed, purified, and crystallized as described previously.[8] Briefly, tetragonal crystals having unit cell dimensions of $a=62$ Å and $c=211$ Å were grown in sitting drops using a reservoir solution of 10% (w/v) Tacsimate, 0.1 M Hepes, pH 7.0, and 19% (w/v) polyethylene glycol (PEG) 3350.[8] The active site of the crystallized enzyme contains a bound L(+)-tartrate ion (*vide infra*), which is a known competitive inhibitor of HAPs.[24,33] The source of the inhibitor is Tacsimate, which contains 0.16 M ammonium tartrate.

The selenomethionine (Se-Met) derivative was created with the Overnight Express Autoinduction System 2 (Novagen). The purification scheme was similar to the one used for native FtHAP. The Se-Met enzyme was crystallized in the Tacsimate/PEG condition with 5 mM dithiothreitol added to the reservoir solution. The resulting crystals are isomorphic to the native ones. Crystals of Se-Met FtHAP were cryoprotected using 25% PEG 200 as described for native FtHAP.[8]

Crystals of the inhibitor-free enzyme were grown using an ammonium-sulfate-based recipe that had been identified previously during crystallization screening trials.[8] These crystals were grown in sitting drops at room temperature using a protein stock solution of 10 mg/mL enzyme in 50 mM sodium acetate, pH 6.0, and reservoir solutions consisting of 0.05–0.2 M Bis–Tris buffer, pH 5.0, and 1.6–2.0 M ammonium sulfate. The crystals are isomorphic to those grown in Tacsimate and PEG.

Crystals used to obtain the complex with P_i were grown using a variation of the PEG/Tacsimate recipe in which Tacsimate was omitted. Large tetragonal crystals were grown in sitting drops at room temperature using reservoir solutions of 0.05–0.20 M Bis–Tris, pH 5.0–6.5, and 17–25% PEG 3350. The P_i complex was formed by soaking a crystal for 30 min in 21% (w/v) PEG 3350, 0.1 M Bis–Tris, pH 6.0, 25% (v/v) PEG 200, and 20 mM P_i (from a stock solution of 100 mM KH_2PO_4 adjusted to pH 6.0). The crystal was then picked up with a Hampton loop and plunged into liquid nitrogen.

Crystals of a substrate-trapping mutant enzyme in which Asp261 is replaced by Ala (D261A) were grown in sitting drops at room temperature using a variation of the ammonium-sulfate-based recipe described above. In this case, the protein stock solution consisted of 15 mg/mL D261A in a buffer of 50 mM sodium acetate at pH 6.0, and the reservoir contained 0.1 M Bis–Tris buffer at pH 6.5 and 2.0 M ammonium sulfate. The complex with the substrate 3′-AMP was formed by soaking a D261A crystal for 45 min in 20 mM 3′-AMP, 2 M ammonium sulfate, 0.1 M Bis–Tris pH 6.5, and 20% (v/v) glycerol prior to freeze-trapping in liquid nitrogen.

X-ray diffraction data collection

Crystals of Se-Met FtHAP were analyzed at beamline 4.2.2 of the Advanced Light Source using a NOIR-1 detector, and the data were processed with D*TREK.[34] The data set that was used for single-wavelength anomalous diffraction (SAD) phasing was collected at the energy corresponding to the peak of f'' ($\lambda=0.97915$ Å). This data set consisted of 360 frames with an oscillation width of 0.5° per image, a detector distance of 150 mm, and an exposure time of 3.5 s/image. The data were processed to 2.10 Å resolution (Table 1).

Data from crystals of the native enzyme were also collected at beamline 4.2.2 and processed with D*TREK (Table 1). The 1.70-Å-resolution data set for the L(+)-tartrate complex was collected using a detector distance of 150 mm and a detector offset angle of 17°. A total of 180° of data were collected using an oscillation angle of 0.5° and an exposure time of 8 s/image. The 1.70-Å-resolution data set for the P_i complex consisted of 180° of data collected with a detector distance of 150 mm, an offset angle of 10°, an oscillation angle of 0.5°, and an exposure time of 3 s/image. The data set used to refine the structure of the inhibitor-free enzyme consisted of 360 images acquired with an oscillation width of 0.5° per image, a detector distance of 160 mm, a detector offset angle of 10°, and an exposure time of 3.5 s/image.

A 1.50-Å-resolution data set was collected from a crystal of the D261A/3′-AMP complex at Northeastern Collaborative Access Team beamline 24-ID-C at the Advanced Photon Source using a Quantum 315 detector. The data set consisted of 180 images collected with a detector distance of 170 mm and an oscillation width of 1°. The data were processed with HKL2000.[35]

Phasing and refinement

The structure was solved using SAD phasing based on data collected from a crystal of Se-Met FtHAP complexed with L(+)-tartrate. SAD phasing calculations were performed with SOLVE[36] using $P4_12_12$ as the space group. Of the expected 12 selenium sites (i.e., one FtHAP molecule per asymmetric unit), 11 were identified, which resulted in a figure of merit of 0.31 for reflections to 2.1 Å resolution. RESOLVE[36] was then used for density modification and automated model building. The phase set from RESOLVE

Please cite this article as: Singh H. *et al.*, Crystal Structures of the Histidine Acid Phosphatase from *Francisella tularensis* Provide Insight into Substrate Recognition, *J. Mol. Biol.* (2009), doi:10.1016/j.jmb.2009.10.009

had a figure of merit of 0.65. The model from automated building included 63% of the expected residues in the asymmetric unit.

REFMAC5[37] and PHENIX[38] were used for refinement. The *B*-factor model used during refinement consisted of an isotropic *B*-factor for each non-hydrogen atom plus one TLS group per chain. Coot[39] was used for model building. The model from RESOLVE was extended through iterative rounds of model building and refinement against the SAD data set to 2.1 Å resolution. The resulting model had an R_{cryst} value of 0.24 and an R_{free} of 0.26. This model served as the starting point for further model building and refinement against the 1.70-Å-resolution native data set for the L(+)-tartrate complex. As the model neared completion, it became apparent that there was a steric clash between two molecules related by the symmetry operation (y, x, $-z$) and involving Met94 and Phe116. This conflict was interpreted as being a violation of $P4_12_12$ symmetry and could be resolved by lowering the symmetry to $P4_1$ and assuming two molecules in the asymmetric unit rather than one. Therefore, subsequent refinement calculations were performed with $P4_1$ as the space group. The final model of the L(+)-tartrate complex was used to initiate refinements of the other structures. A common set of test reflections (5%) was used for all the refinements. See Table 1 for refinement statistics.

Site-directed mutagenesis

Three site-directed mutants of FtHAP—in which Ala replaced Phe23 (F23A), Tyr135 (Y135A), or Asp261 (D261A)—were created. These alterations to the FtHAP gene were made using the overlap extension PCR method as originally described by Horton *et al.*[40,41] PCR cycling parameters for generation of the overlap amplicons were as follows: initial denaturation at 94 °C for 60 s followed by 30 cycles of 94 °C denaturation (30 s), annealing at 55 °C (60 s), and elongation at 72 °C (120 s). The blunt-ended final PCR product was cloned into pZERO Blunt, transformed into *Escherichia coli* DH5α, and cultured on LB containing 50 μg/mL kanamycin. The blunt insert was ligated into pET20b using NcoI and XhoI restriction sites. The mutant enzymes were expressed and purified using protocols similar to those described above for the native enzyme.

Kinetic characterization

Initial kinetic screening trials identified 3′-AMP and *p*-nitrophenyl phosphate (*p*NPP) as two of the best *in vitro* substrates for FtHAP (Supplementary Fig. S1); therefore, these molecules were used for characterization of steady-state kinetics. Enzymatic activity with 3′-AMP as the substrate was assessed using a discontinuous assay that measures the production of P_i.[42,43] The assays were performed at 37 °C in a buffer of 0.2 M sodium acetate at pH 6.0. We note that FtHAP exhibits negligible activity at pH values greater than 7.0 with *p*NPP as the substrate, suggesting that the enzyme can be considered to be an acid phosphatase (data not shown). For each substrate concentration, the reaction was stopped by the addition of the malachite green reagent after reaction times of 15, 30, 45, and 60 s, and the P_i concentrations were then determined spectrophotometrically. The initial rate was estimated by fitting data from the four time points to a line. The kinetic constants K_m and V_{max} were estimated by fitting the initial rate data to the Michaelis–Menten equation using Origin 8 software. Inhibition by L(+)-tartrate was studied using *p*NPP as the substrate at 37 °C in a buffer of 0.2 M sodium acetate at pH 6.0. In this case, the production of *p*-nitrophenolate was monitored at 405 nm as described previously.[10] The inhibition constant (K_i) was estimated using simultaneous nonlinear regression as described by Kakkar *et al.*[44]

Accession codes

Atomic coordinates and structure factor amplitudes have been deposited in the PDB[45] with accession codes 3IT0, 3IT1, 3IT2, and 3IT3.

Acknowledgements

We thank Dr. Michael Calcutt for help with mutagenesis experiments. We thank Dr. Jay Nix of Advanced Light Source (ALS) beamline 4.2.2 for help with data collection. This research was supported by National Institutes of Health (NIH) grant U54 AI057160 to the Midwest Regional Center of Excellence for Biodefense and Emerging Infectious Disease Research and the University of Missouri Research Board. H.S. was supported by a predoctoral fellowship from NIH grant DK071510. Part of this research was performed at the ALS. The ALS is supported by the Director, Office of Science, Office of Basic Energy Sciences of the U.S. Department of Energy under Contract No. DE-AC02-05CH11231. Part of this work is based upon research conducted at the Northeastern Collaborative Access Team beamlines of the Advanced Photon Source, supported by award RR-15301 from the National Center for Research Resources at the NIH. Use of the Advanced Photon Source is supported by the U.S. Department of Energy, Office of Basic Energy Sciences, under Contract No. W-31-109-ENG-38.

Supplementary Data

Supplementary data associated with this article can be found, in the online version, at doi:10.1016/j.jmb.2009.10.009

References

1. Oyston, P. C., Sjostedt, A. & Titball, R. W. (2004). Tularaemia: bioterrorism defence renews interest in *Francisella tularensis*. *Nat. Rev., Microbiol.* **2**, 967–978.
2. Mohapatra, N. P., Balagopal, A., Soni, S., Schlesinger, L. S. & Gunn, J. S. (2007). AcpA is a *Francisella* acid phosphatase that affects intramacrophage survival and virulence. *Infect. Immun.* **75**, 390–396.
3. Mohapatra, N. P., Soni, S., Reilly, T. J., Liu, J., Klose, K. E. & Gunn, J. S. (2008). Combined deletion of four *Francisella novicida* acid phosphatases attenuates virulence and macrophage vacuolar escape. *Infect. Immun.* **76**, 3690–3699.
4. Felts, R. L., Reilly, T. J. & Tanner, J. J. (2006). Structure of *Francisella tularensis* AcpA: prototype of a unique

superfamily of acid phosphatases and phospholipases C. *J. Biol. Chem.* **281**, 30289–30298.
5. Singh, H., Felts, R. L., Ma, L., Malinski, T. J., Calcutt, M. J., Reilly, T. J. & Tanner, J. J. (2009). Expression, purification and crystallization of class C acid phosphatases from *Francisella tularensis* and *Pasteurella multocida*. *Acta Crystallogr., Sect. F*, **65**, 226–231.
6. Rossolini, G. M., Schippa, S., Riccio, M. L., Berlutti, F., Macaskie, L. E. & Thaller, M. C. (1998). Bacterial nonspecific acid phosphohydrolases: physiology, evolution and use as tools in microbial biotechnology. *Cell. Mol. Life Sci.* **54**, 833–850.
7. Felts, R. L., Reilly, T. J. & Tanner, J. J. (2005). Crystallization of AcpA, a respiratory burst-inhibiting acid phosphatase from *Francisella tularensis*. *Biochim. Biophys. Acta*, **1752**, 107–110.
8. Felts, R. L., Reilly, T. J., Calcutt, M. J. & Tanner, J. J. (2006). Crystallization of a newly discovered histidine acid phosphatase from *Francisella tularensis*. *Acta Crystallogr., Sect. F*, **62**, 32–35.
9. Reilly, T. J., Baron, G. S., Nano, F. E. & Kuhlenschmidt, M. S. (1996). Characterization and sequencing of a respiratory burst-inhibiting acid phosphatase from *Francisella tularensis*. *J. Biol. Chem.* **271**, 10973–10983.
10. Reilly, T. J., Felts, R. L., Henzl, M. T., Calcutt, M. J. & Tanner, J. J. (2006). Characterization of recombinant *Francisella tularensis* acid phosphatase A. *Protein Expr. Purif.* **45**, 132–141.
11. Van Etten, R. L., Davidson, R., Stevis, P. E., MacArthur, H. & Moore, D. L. (1991). Covalent structure, disulfide bonding, and identification of reactive surface and active site residues of human prostatic acid phosphatase. *J. Biol. Chem.* **266**, 2313–2319.
12. Jakob, C. G., Lewinski, K., Kuciel, R., Ostrowski, W. & Lebioda, L. (2000). Crystal structure of human prostatic acid phosphatase. *Prostate*, **42**, 211–218.
13. LaCount, M. W., Handy, G. & Lebioda, L. (1998). Structural origins of L(+)-tartrate inhibition of human prostatic acid phosphatase. *J. Biol. Chem.* **273**, 30406–30409.
14. Ortlund, E., LaCount, M. W. & Lebioda, L. (2003). Crystal structures of human prostatic acid phosphatase in complex with a phosphate ion and alpha-benzylaminobenzylphosphonic acid update the mechanistic picture and offer new insights into inhibitor design. *Biochemistry*, **42**, 383–389.
15. Lindqvist, Y., Schneider, G. & Vihko, P. (1993). Three-dimensional structure of rat acid phosphatase in complex with L(+)-tartrate. *J. Biol. Chem.* **268**, 20744–20746.
16. Lindqvist, Y., Schneider, G. & Vihko, P. (1994). Crystal structures of rat acid phosphatase complexed with the transition-state analogs vanadate and molybdate. Implications for the reaction mechanism. *Eur. J. Biochem.* **221**, 139–142.
17. Schneider, G., Lindqvist, Y. & Vihko, P. (1993). Three-dimensional structure of rat acid phosphatase. *EMBO J.* **12**, 2609–2615.
18. Engh, R. A. & Huber, R. (1991). Accurate bond and angle parameters for x-ray protein structure refinement. *Acta Crystallogr., Sect. A: Found. Crystallogr.* **47**, 392–400.
19. Lovell, S. C., Davis, I. W., Arendall, W. B., III, de Bakker, P. I., Word, J. M., Prisant, M. G. *et al.* (2003). Structure validation by C^{α} geometry: phi,psi and C^{β} deviation. *Proteins*, **50**, 437–450.
20. DeLano, W. L. (2002). The PyMOL User's Manual DeLano Scientific, Palo Alto, CA.
21. Rigden, D. J. (2008). The histidine phosphatase superfamily: structure and function. *Biochem. J.* **409**, 333–348.
22. Krissinel, E. & Henrick, K. (2003). 5th International Conference on Molecular Structural Biology, Vienna, Austria.
23. Krissinel, E. & Henrick, K. (2007). Inference of macromolecular assemblies from crystalline state. *J. Mol. Biol.* **372**, 774–797.
24. Ostanin, K., Saeed, A. & Van Etten, R. L. (1994). Heterologous expression of human prostatic acid phosphatase and site-directed mutagenesis of the enzyme active site. *J. Biol. Chem.* **269**, 8971–8978.
25. Ostanin, K. & Van Etten, R. L. (1993). Asp304 of *Escherichia coli* acid phosphatase is involved in leaving group protonation. *J. Biol. Chem.* **268**, 20778–20784.
26. Flint, A. J., Tiganis, T., Barford, D. & Tonks, N. K. (1997). Development of "substrate-trapping" mutants to identify physiological substrates of protein tyrosine phosphatases. *Proc. Natl Acad. Sci. USA*, **94**, 1680–1685.
27. Meng, T. C. & Lin, M. F. (1998). Tyrosine phosphorylation of c-ErbB-2 is regulated by the cellular form of prostatic acid phosphatase in human prostate cancer cells. *J. Biol. Chem.* **273**, 22096–22104.
28. Lin, M. F. & Clinton, G. M. (1988). The epidermal growth factor receptor from prostate cells is dephosphorylated by a prostate-specific phosphotyrosyl phosphatase. *Mol. Cell. Biol.* **8**, 5477–5485.
29. Sowa, N. A., Vadakkan, K. I. & Zylka, M. J. (2009). Recombinant mouse PAP Has pH-dependent ectonucleotidase activity and acts through A(1)-adenosine receptors to mediate antinociception. *PLoS ONE*, **4**, e4248.
30. Zylka, M. J., Sowa, N. A., Taylor-Blake, B., Twomey, M. A., Herrala, A., Voikar, V. & Vihko, P. (2008). Prostatic acid phosphatase is an ectonucleotidase and suppresses pain by generating adenosine. *Neuron*, **60**, 111–122.
31. Rigden, D. J., Mello, L. V., Setlow, P. & Jedrzejas, M. J. (2002). Structure and mechanism of action of a cofactor-dependent phosphoglycerate mutase homolog from *Bacillus stearothermophilus* with broad specificity phosphatase activity. *J. Mol. Biol.* **315**, 1129–1143.
32. Aragon, V., Kurtz, S. & Cianciotto, N. P. (2001). *Legionella pneumophila* major acid phosphatase and its role in intracellular infection. *Infect. Immun.* **69**, 177–185.
33. Van Etten, R. L. & Saini, M. S. (1978). Selective purification of tartrate-inhibitable acid phosphatases: rapid and efficient purification (to homogeneity) of human and canine prostatic acid phosphatases. *Clin. Chem.* **24**, 1525–1530.
34. Pflugrath, J. W. (1999). The finer things in X-ray diffraction data collection. *Acta Crystallogr., Sect. D: Biol. Crystallogr.* **55**, 1718–1725.
35. Otwinowski, Z. & Minor, W. (1997). Processing of X-ray diffraction data collected in oscillation mode. *Methods Enzymol.* **276**, 307–326.
36. Terwilliger, T. C. (2003). SOLVE and RESOLVE: automated structure solution and density modification. *Methods Enzymol.* **374**, 22–37.
37. Murshudov, G. N., Vagin, A. A. & Dodson, E. J. (1997). Refinement of macromolecular structures by the maximum-likelihood method. *Acta Crystallogr., Sect. F*, **53**, 240–255.
38. Adams, P. D., Gopal, K., Grosse-Kunstleve, R. W., Hung, L. W., Ioerger, T. R., McCoy, A. J. *et al.* (2004). Recent developments in the PHENIX software for automated crystallographic structure determination. *J. Synchrotron Radiat.* **11**, 53–55.

Please cite this article as: Singh H. *et al.*, Crystal Structures of the Histidine Acid Phosphatase from *Francisella tularensis* Provide Insight into Substrate Recognition, *J. Mol. Biol.* (2009), doi:10.1016/j.jmb.2009.10.009

39. Emsley, P. & Cowtan, K. (2004). Coot: model-building tools for molecular graphics. *Acta Crystallogr., Sect. D: Biol. Crystallogr.* **60**, 2126–2132.
40. Horton, R. M., Cai, Z. L., Ho, S. N. & Pease, L. R. (1990). Gene splicing by overlap extension: tailor-made genes using the polymerase chain reaction. *BioTechniques*, **8**, 528–535.
41. Horton, R. M., Hunt, H. D., Ho, S. N., Pullen, J. K. & Pease, L. R. (1989). Engineering hybrid genes without the use of restriction enzymes: gene splicing by overlap extension. *Gene*, **77**, 61–68.
42. Lanzetta, P. A., Alvarez, L. J., Reinach, P. S. & Candia, O. A. (1979). An improved assay for nanomole amounts of inorganic phosphate. *Anal. Biochem.* **100**, 95–97.
43. Carter, S. G. & Karl, D. W. (1982). Inorganic phosphate assay with malachite green: an improvement and evaluation. *J. Biochem. Biophys. Methods*, **7**, 7–13.
44. Kakkar, T., Boxenbaum, H. & Mayersohn, M. (1999). Estimation of K_i in a competitive enzyme-inhibition model: comparisons among three methods of data analysis. *Drug Metab. Dispos.* **27**, 756–762.
45. Berman, H. M., Westbrook, J., Feng, Z., Gilliland, G., Bhat, T. N., Weissig, H. *et al.* (2000). The Protein Data Bank. *Nucleic Acids Res.* **28**, 235–242.

Please cite this article as: Singh H. *et al.*, Crystal Structures of the Histidine Acid Phosphatase from *Francisella tularensis* Provide Insight into Substrate Recognition, *J. Mol. Biol.* (2009), doi:10.1016/j.jmb.2009.10.009